ELSEVIER

Fluid Phase Equilibria 200 (2002) 121–145

FLUID PHASE EQUILIBRIA

www.elsevier.com/locate/fluid

Computer simulations and crossover equation of state of square-well fluids

S.B. Kiselev [a,*], J.F. Ely [a], L. Lue [b], J.R. Elliott, Jr. [c]

[a] *Chemical Engineering Department, Colorado School of Mines, 1500 Illinois Street, Golden, CO 80401-1887, USA*
[b] *Department of Chemical Engineering, UMIST, P.O. Box 88, Manchester M60 1QD, UK*
[c] *Chemical Engineering Department, The University of Akron, Akron, OH 44325-3906, USA*

Received 27 February 2001; accepted 9 January 2002

Abstract

We develop a crossover equation of state (EOS) for square-well fluids with varying well width. This equation yields the exact second and third virial coefficients, and accurately reproduces first-order (high-temperature) perturbation theory results. In addition, this EOS yields the correct scaling exponents near the critical point. We perform extensive new molecular dynamics and Monte Carlo simulations in the one-phase region for varying well widths of $\lambda = 1.5$, 2.0, and 3.0. We fit the parameters of our EOS to one-phase and two-phase thermodynamic data from our simulations and those of previous researchers. The resulting EOS is found to represent the thermodynamic properties of these square-well fluids to less than 1% deviation in internal energy and density and 0.1% deviation in vapor pressure.

Keywords: Computer simulations; Critical point; Crossover theory; Equation-of-state; Square-well fluids; Thermodynamic properties; Vapor–liquid equilibria

1. Introduction

Because of its simplicity, the square-well fluid has long served as a model system for understanding the behavior of real fluids. The interaction energy $u(r)$ between two square-well molecules separated by a distance r is given by

$$u(r) = \begin{cases} +\infty, & \text{for } r < \sigma \\ -\epsilon, & \text{for } \sigma < r < \lambda\sigma \\ 0, & \text{for } \lambda\sigma < r \end{cases} \tag{1}$$

where σ is the diameter of the hard-sphere repulsive interaction, ϵ is the strength of the attractive interaction, and λ characterizes the range of the attractive interaction. This model interaction possesses

* Corresponding author. Tel.: +1-303-273-3190; fax: +1-303-273-3730.
E-mail address: skiselev@mines.edu (S.B. Kiselev).

0378-3812/02/$ – see front matter
PII: S0378-3812(02)00022-5

the basic interactions found in many real fluids: a short-range attractive interaction and a repulsive excluded volume interactions. As a result, it possesses all the complex behavior of real fluid systems.

Due to its importance, the thermodynamic properties of the square-well fluid have been extensively studied using computer simulation methods in both the one-phase region [1–8] and the two-phase region [9–11]. There has also been a lot of work in trying to obtain an equation of state (EOS) for variable-width square-well fluids.

One approach has been to construct empirical forms and to fit the parameters to available simulation data [12–14]. Unfortunately, in these previous works, the empirical forms did not incorporate known theoretical results (e.g. the second and third virial coefficients, the scaling behavior near the critical point, etc.), and as a result their accuracy is limited.

Another approach that has been taken is to take the hard-sphere fluid as a reference system and to use perturbation theory around the high-temperature limit to obtain the properties of the square-well fluid [12]. In this approach, the coefficients of the perturbation expansion have been obtained through empirical fits to simulation data [2,12,15–17], approximate theories for the hard-sphere correlation functions [18,19], expansion around the $\lambda \rightarrow \infty$ limit [20], and expansion around the $\lambda \rightarrow 1$ limit [21,22].

A simpler description of the square-well fluid, based on the lattice theory of fluids, is given by the quasi-chemical approximation [4,5,8,23–27]. The advantage of these approaches is that they lead to simple analytical forms for the free energy of the system. However, the predictions of the quasi-chemical approximation are not very accurate.

Integral equation approaches have also been employed with various approximate closure relations, including the Percus–Yevick [28], hypernetted chain [1], mean spherical approximation [29], and hybrid mean-spherical approximation closures [30]. Although these methods are theoretically based, they still do not reproduce all the known behaviors of the square-well fluid.

One of the common difficulties with the theoretical approaches is that they do not properly describe the critical region. Attempts have been made to construct crossover equations of state for square-well fluids which do yield nonclassical scaling behavior near the critical point [31–33]. However, in these approaches, the critical scaling exponents are only correct to first-order in the epsilon expansion, and do not yield the correct scaling of the caloric properties of the system. For example, the predicted isochoric heat capacity near the critical point is not divergent (i.e. $\alpha = 0$), in contrast to what is expected theoretically (i.e. $\alpha \approx 0.110$).

In this work, we attempt to construct a semi-empirical EOS for square-well fluids which will accurately represent the thermodynamic properties of variable-width square-well fluids at all state points. The form of the EOS is constructed such that it yields the exact second and third virial coefficients, and also reproduces the first-order high-temperature coefficient. In addition, near the critical point this EOS also possesses the correct scaling form.

The remainder of this paper is organized as follows. In Section 2, we describe our classical EOS for square-well fluids. In Section 3, we formulate a new crossover formulation. This new formulation, unlike previous ones, is well behaved far from the critical point, even in the infinite temperature limit. We combine our classical EOS with this new crossover formulation. In Section 4, we provide the details for our Monte Carlo and molecular dynamics simulations for square-well fluids. In Section 5, we fit the parameters for our new crossover EOS to available simulation data for square-well fluids. In Section 6, we summarize the major findings of this paper.

2. Classical free energy

The residual Helmholtz free energy A^{res} of a square-well system can be divided into a contribution from the hard-sphere interactions A^{HS} and a contribution from the attractive interactions A^{att}

$$A^{\mathrm{res}} = A^{\mathrm{HS}} + A^{\mathrm{att}} \tag{2}$$

For the free energy of a hard-sphere system, we use the Carnahan–Starling EOS [34], which has been shown to accurately represent the thermodynamic properties of the hard-sphere fluid. Note that this EOS possesses the exact second and third virial coefficients.

The behavior of the attractive contribution to the Helmholtz free energy is fairly complex, and many forms have been proposed to describe it. To get a feeling for how to model this term, we examine the behavior of A^{att} in the low-density limit. In this regime, the Helmholtz free energy can be accurately represented by a virial series

$$\frac{A^{\mathrm{att}}}{Nk_{\mathrm{B}}T} = B_2^{\mathrm{att}}\rho + \tfrac{1}{2}B_3^{\mathrm{att}}\rho^2 + \cdots \tag{3}$$

where $B_n^{\mathrm{att}} = B_n - B_n^{\mathrm{HS}}$ is the attractive contribution to the nth virial coefficient, B_n the nth virial coefficient of the square-well fluid, and B_n^{HS} is the nth virial coefficient of the hard-sphere fluid. For the square-well fluid, the second and third virial coefficients are known exactly [35]

$$B_2 = B_2^{\mathrm{HS}}[1 - (\lambda^3 - 1)\Delta] \tag{4}$$

$$B_3 = B_3^{\mathrm{HS}}[1 - f_1(\lambda)\Delta - f_2(\lambda)\Delta^2 - f_3(\lambda)\Delta^3] \tag{5}$$

where $\Delta = \exp[\epsilon/(k_{\mathrm{B}}T)] - 1$, and

$$f_1(\lambda) = \begin{cases} 0, & \text{for } \lambda \le 1 \\ \frac{1}{5}(\lambda^6 - 18\lambda^4 + 32\lambda^3 - 15), & \text{for } 1 < \lambda < 2 \\ \frac{17}{5}, & \text{for } 2 < \lambda \end{cases} \tag{6}$$

$$f_2(\lambda) = \begin{cases} 0, & \text{for } \lambda \le 1 \\ \frac{2}{5}(\lambda^6 - 18\lambda^4 + 16\lambda^3 + 9\lambda^2 - 8), & \text{for } 1 < \lambda < 2 \\ \frac{1}{5}(-32\lambda^3 + 18\lambda^2 + 48), & \text{for } 2 < \lambda \end{cases} \tag{7}$$

$$f_3(\lambda) = \begin{cases} 0, & \text{for } \lambda \le 1 \\ \frac{6}{5}(\lambda^2 - 1)^3, & \text{for } 1 < \lambda < 2 \\ \frac{1}{5}(5\lambda^6 - 32\lambda^3 + 18\lambda^2 + 26), & \text{for } 2 < \lambda \end{cases} \tag{8}$$

In this limit, we see that each of the virial coefficients is a polynomial function of Δ.

Taking this into consideration, we propose the following empirical form for A^{att}

$$\frac{A^{\mathrm{att}}}{Nk_{\mathrm{B}}T} = -A_0 \ln(1 + A_1\Delta + A_2\Delta^2 + A_3\Delta^3) \tag{9}$$

where N is the number of particles in the system, k_B the Boltzmann constant, T is the absolute temperature of the system, and the functions A_0, A_1, A_2, and A_3 are given by Pade approximants [36]

$$A_0 = \frac{a_0^{(0)} + a_0^{(2)} y^2 + a_0^{(3)} y^3 + a_0^{(5)} y^5}{1 + b_0^{(2)} y^2} \tag{10}$$

$$A_1 = \frac{1}{A_0}\left[\frac{a_1^{(1)} y}{1 + b_1^{(1)} y + b_1^{(2)} y^2 + b_1^{(3)} y^3}\right] \tag{11}$$

$$A_2 = \frac{a_2^{(2)} y^2 + a_2^{(3)} y^3}{1 + b_2^{(1)} y + b_2^{(2)} y^2 + b_2^{(3)} y^3} \tag{12}$$

$$A_3 = \frac{a_3^{(2)} y^2 + a_3^{(3)} y^3}{1 + b_3^{(1)} y + b_3^{(2)} y^2 + b_3^{(3)} y^3} \tag{13}$$

where $y = \pi\sigma^3\rho/6$ is the packing fraction of the spheres, and ρ is the number density of spheres. The application of the logarithmic form for the attractive free energy was motivated by the forms of the Redlich–Kwong and Peng–Robinson engineering equations, and by the observation that the predominant density dependence seems to soften for high density square-well fluids.

Expanding Eq. (9) around zero density and comparing the result with the virial series, we find the following relations

$$a_1^{(1)} = 4(\lambda^3 - 1) \tag{14}$$

$$b_1^{(1)} = -\frac{5}{4}\frac{f_1(\lambda)}{(\lambda^3 - 1)} \tag{15}$$

$$a_2^{(2)} = \frac{1}{a_0^{(0)}}\left[8(\lambda^3 - 1) + \frac{1}{a_0^{(0)}} 5 f_2(\lambda)\right] \tag{16}$$

$$a_3^{(2)} = \frac{1}{a_0^{(0)}} 5 f_3(\lambda) \tag{17}$$

By using these relations for the coefficients, the resulting free energy will possess the exact second and third virial coefficients.

At high-temperatures, the free energy can be expanded as

$$\frac{A^{\text{att}}}{N k_B T} = A_1'\left(\frac{\epsilon}{k_B T}\right) + A_2'\left(\frac{\epsilon}{k_B T}\right)^2 + \cdots \tag{18}$$

where the coefficients A_n' can be determined from only the properties of the hard-sphere fluid.

For example, the coefficient A_1' can be obtained from the pair correlation function of the hard-sphere system g_{HS}

$$A_1' = 2\pi\rho \int_\sigma^{\lambda\sigma} \mathrm{d}r\, r^2 g_{\text{HS}}(r) \tag{19}$$

By expanding our free energy about the infinite temperature (i.e. $\epsilon/k_BT = 0$) limit, we find

$$A_1' = A_0 A_1$$

In order to reproduce the correct first-order perturbation term A_1', we fit the parameters $b_1^{(2)}$ and $b_1^{(3)}$ to the results of Eq. (19), with $g_{HS}(r)$ computed by the Verlet–Weis [37] procedure. This fit results in average deviations from A_1' of less than 0.2%, as discussed in Section 5.

In the critical region, the dimensionless Helmholtz free energy $\bar{A}(T, v) = A(T, v)/k_BT$ can be split into the two parts

$$\bar{A}(T, v) = \Delta\bar{A}(\tau, \varphi) + \bar{A}_{reg}(T, v) \tag{20}$$

where the critical, or singular part of the free energy, $\Delta\bar{A}$ is a function of the dimensionless temperature deviation $\tau = T/T_c - 1$ and the order parameter φ, while the regular part $\bar{A}_{reg}(T, v)$ is a smooth, analytic function of the temperature T and the molar volume $v = V/N$. For the classical EOS, the critical part $\Delta\bar{A}(\tau, \varphi)$ is an analytic function of the variables and, asymptotically close to the critical point (where $|\tau| \ll 1$ and $|\varphi| \ll 1$), can be represented by a Taylor expansion

$$\Delta\bar{A}(\tau, \varphi) = a_{12}\tau\varphi^2 + a_{04}\varphi^4 \tag{21}$$

that corresponds to the Landau, or mean-field (MF), theory of critical phenomena [38]. In simple fluids, a dimensionless deviation of the density ρ or the molar volume v from its critical value (or their combination) [39], can be chosen as the order parameter, and the quantity $h = (\partial\Delta\bar{A}/\partial\varphi)_\tau$, conjugate to the order parameter φ, plays the role of the ordering field. From the condition $h = 0$ at $\tau \leq 0$, we have that the equilibrium value of the order parameter on the coexistence curve $\varphi_{cxs} \propto |\tau|^{1/2}$. For $\tau > 0$, the condition $h = 0$ corresponds to the condition $\varphi = 0$, the susceptibility $\bar{\chi}_\tau = (\partial\varphi/\partial h)_\tau \propto \tau^{-1}$, and the singular part of the isochoric heat capacity $\Delta\bar{C}_V = -(\partial^2\Delta\bar{A}/\partial\tau^2)_V$ remains constant as $|\tau| \to 0$. Thus, for any classical EOS, the critical exponents

$$\beta_L = \tfrac{1}{2}, \qquad \gamma_L = 1, \qquad \alpha_L = 0. \tag{22}$$

The MF behavior is valid only in the region where the large-scale fluctuations of the order parameter are negligibly small. The size of this region is characterized by the Ginzburg number (Gi) [40]

$$Gi = \kappa\left(\frac{\bar{l}}{\bar{l}_0}\right)^6 \tag{23}$$

where κ is a numerical constant which in general depends on the path of approach to the critical point and the property of interest, $\bar{l}$ is an average distance between particles, and $\bar{l}_0$ is an effective radius of the interaction between molecules. At zero ordering field ($h = 0$), which in the simple fluids corresponds to the critical isochore ($v = v_c$) at $\tau \geq 0$ or to the coexistence curve ($v = v_{L,V}$) at $\tau < 0$, the Landau theory is valid only in the temperature region

$$Gi \ll |\tau| \ll 1. \tag{24}$$

As the critical point is approached ($T \to T_c$), at temperatures

$$|\tau| \ll Gi, \tag{25}$$

the intensity of the long-range fluctuations of the order parameter anomalously increases and diverges at the critical point. As a consequence, at these temperatures the critical part of the thermodynamic

potential $\Delta\bar{A}$ becomes a non-analytic, scaling function of the dimensionless temperature τ and the order parameter φ. At zero ordering field, the asymptotic singular behavior of the thermodynamic properties can be described in terms of scaling laws [41,42]

$$\varphi_{\rm cxs} = \pm B_0|\tau|^{\beta}(1 + B_1|\tau|^{\Delta_1}), \quad \bar{\chi}_\tau = \Gamma_0^{\pm}|\tau|^{-\gamma}(1 + \Gamma_1|\tau|^{\Delta_1}), \quad \Delta\bar{C}_V = A_0^{\pm}|\tau|^{-\alpha}(1 + A_1|\tau|^{\Delta_1}) \tag{26}$$

where signs '±' correspond to the liquid (+) and vapor (−) phases, the superscripts '±' correspond to the high ($T > T_{\rm c}$) and low ($T < T_{\rm c}$) temperature regions, the subscripts '0' and '1' correspond to the asymptotic and first Wegner correction terms, respectively, and the universal critical exponents

$$\beta = 0.325, \qquad \gamma = 1.24, \qquad \alpha = 2 - \gamma - 2\beta = 0.110, \qquad \Delta_1 = 0.51. \tag{27}$$

In order to describe the crossover from the MF behavior (with the critical exponents given by Eq. (22)) to the asymptotic scaling behavior (given by Eq. (26)), the crossover theory should be applied [43,44]. We describe this procedure in the following section.

3. Crossover free energy

A general procedure for transforming any classical EOS into the crossover form was proposed by Kiselev [45]. This procedure has a theoretical foundation in the renormalization-group (RG) theory and has been successfully applied to the cubic Patel–Teja (PT) EOS [45,46] and to the statistical associating fluid theory (SAFT) EOS [47,48]. Following this method, we first rewrite the classical expression (20) for the Helmholtz free energy in dimensionless form

$$\bar{A}(T, v) = \Delta\bar{A}(\tau, \varphi) - \varphi\bar{P}_0(T) + \bar{A}_0^{\rm res}(T) + \bar{A}_0(T), \tag{28}$$

where we use the definition $\varphi = v/v_{\rm c} - 1$. $\bar{P}_0(T) = P(T, v_{\rm c})v_{\rm c}/k_{\rm B}T$ is the dimensionless pressure, $\bar{A}_0^{\rm r}(T) = A^{\rm res}(T, v_{\rm c})/k_{\rm B}T$ is the dimensionless residual part of the Helmholtz free energy along the critical isochore, and $\bar{A}_0(T) = A_0(T)/k_{\rm B}T$ is the dimensionless temperature-dependent part of the ideal gas Helmholtz free energy. The critical part of the dimensionless Helmholtz free energy is

$$\Delta\bar{A}(\tau, \varphi) = \bar{A}^{\rm res}(\tau, \varphi) - \bar{A}^{\rm res}(\tau, 0) - \ln(\varphi + 1) + \varphi\bar{P}_0(\tau), \tag{29}$$

where $\bar{A}^{\rm res} = A^{\rm res}/k_{\rm B}T$ is the dimensionless residual part of the Helmholtz free energy.

Secondly, we replace τ and φ in the critical part of the classical Helmholtz free energy $\Delta\bar{A}$ in Eq. (28) by the renormalized values [45]

$$\bar{\tau} = \tau Y^{-\alpha/2\Delta_1}, \qquad \bar{\varphi} = \varphi Y^{(\gamma-2\beta)/4\Delta_1}, \tag{30}$$

where Y is a crossover function to be specified below and the critical exponents are given by Eq. (27). Eq. (30) corresponds to the formal solution of the renormalization-group equations obtained near the actual critical point of the system with the real critical temperature $T_{\rm c}$ and critical volume $v_{\rm c}$. In general, these critical parameters do not coincide with the classical critical parameters $T_{0\rm c}$ and $v_{0\rm c}$ which are found from the classical SW EOS (2) through the conditions

$$P_{\rm c} = -\left(\frac{\partial A}{\partial v}\right)_{T_{0\rm c}}, \qquad \left(\frac{\partial^2 A}{\partial v^2}\right)_{T_{0\rm c}} = 0, \qquad \left(\frac{\partial^3 A}{\partial v^3}\right)_{T_{0\rm c}} = 0. \tag{31}$$

These equations for the SW EOS can only be solved numerically, and, in general, T_{0c}, v_{0c}, and P_{0c} are complicated functions of the parameters $a_j^{(i)}$ and $b_j^{(i)}$. Therefore, in order to take into account the difference between the classical and real critical parameters of the SW fluid, following Kiselev [45], we have introduced in Eq. (30) the additional terms

$$\bar{\tau} = \tau Y^{-\alpha/2\Delta_1} + (1+\tau)\Delta\tau_c Y^{2(2-\alpha)/3\Delta_1}, \tag{32}$$

$$\bar{\varphi} = \varphi Y^{(\gamma-2\beta)/4\Delta_1} + (1+\varphi)\Delta\varphi_c Y^{(2-\alpha)/2\Delta_1}, \tag{33}$$

where $\Delta\tau_c = (T_c - T_{0c})/T_{0c} = \Delta T_c/T_{0c}$ and $\Delta\varphi_c = (v_c - v_{0c})/v_{0c} = \Delta v_c/v_{0c}$ are the dimensionless shifts of the critical temperature and the critical volume, respectively. If the real critical parameters of the system T_c and v_c are known, then the critical shifts $\Delta\tau_c$ and $\Delta\varphi_c$ are also known. Otherwise, following Kiselev and Ely [48] one can represent the critical shifts as functions of the Gi

$$\Delta\tau_c = -\frac{\delta_\tau Gi}{1+Gi}, \qquad \Delta\varphi_c = -\frac{\delta_\varphi Gi}{1+Gi}, \tag{34}$$

where the coefficients δ_τ and δ_φ do not depend on the parameters of the intermolecular potential and for the classical EOS of interest can be treated as constants. For this approach to be feasible, $\Delta\tau_c \ll 1$ and $\Delta\varphi_c \ll 1$. Note that preliminary applications of perturbation theory in place of Eq. (9) resulted in values of $\Delta\tau_c$ and $\Delta\varphi_c$ that were too large, motivating the need for more empirical parameters, as exhibited in Eq. (9).

In order to complete transformation, one needs to add in Eq. (28) the kernel term

$$\mathcal{K}(\tau^2) = \frac{1}{2}a_{20}\left(\frac{\tau}{\tau+1}\right)^2 (Y^{-\alpha/\Delta_1} - 1), \tag{35}$$

which provides the correct scaling behavior of the isochoric specific heat asymptotically close to the critical point. We need to note, that the kernel term as given by Eq. (35) differs slightly from the corresponding kernel term employed earlier by Kiselev [45]. In order to avoid the unphysical divergence as $\tau \to \infty$, we replaced the prefactor τ^2 in the kernel term in [45] with the function $\tau^2/(\tau+1)^2$. In the critical region, at $\tau \ll 1$, the function $\tau^2/(\tau+1)^2 \cong \tau^2$, and both terms practically coincide. As $|\tau| \gg 1$, the crossover function $Y(q) \to 1$, so $\mathcal{K} \to 0$.

The crossover function Y in Eqs. (30) and (35) can be written in parametric form [45]

$$Y(q) = [q/R(q)]^{\Delta_1}, \tag{36}$$

where here, unlike the previous crossover model [45], for the function $R(q)$ we adopted the Pade-approximant of the numerical solution of the RG equations [49,50]

$$R(q) = 1 + \frac{q^2}{q+1}. \tag{37}$$

In Eq. (36) the parametric variable $q = r/Gi$, where r is a dimensionless measure of the distance from the critical point, which at the critical isochore coincides with the dimensionless temperature deviation τ [43–45]. In the original Kiselev approach [45], the variable r was determined from a solution of the parametric linear-model (LM) EOS. The LM EOS has a theoretical foundation in the renormalization-group theory [51], but it cannot be extended into the metastable region and represent analytically connected van der Waals loops. Therefore, in the present work, we find the parametric variable r from a solution

of the parametric sine-model developed recently by Fisher et al. [52] and represented in crossover form by Kiselev and Ely [48]. With account of the redefinition of the function $R(q)$ adopted in this work, the crossover sine-model equation for the variable q can be written in the form

$$\left(q - \frac{\tau}{Gi}\right)\left[1 - \frac{p^2}{4b^2}\left(1 - \frac{\tau}{qGi}\right)\right] = b^2\left(\frac{\varphi}{m_0 Gi^{\beta}}\right)^2 Y(q)^{(1-2\beta)/\Delta_1}, \tag{38}$$

where m_0 is a system-dependent parameters, and $p^2 = b^2 = 1.359$ are the universal sine-, p^2-, and linear-model, b^2, parameters [48]. The linear-model crossover equation for the parametric variable q employed earlier by Kiselev [49] is recaptured from Eq. (38) when the sine-model parameter $p^2 \to 0$.

Finally, the crossover expression for the Helmholtz free energy can be written in the form

$$\begin{aligned}\bar{A}(T, v) = {} & \bar{A}^{\mathrm{res}}(\bar{\tau}, \bar{\varphi}) - \bar{A}^{\mathrm{res}}(\bar{\tau}, 0) - \ln(\bar{\varphi} + 1) + \bar{\varphi}\bar{P}_0(\bar{\tau}) \\ & - \Delta v \bar{P}_0(T) + \bar{A}_0^{\mathrm{res}}(T) + \bar{A}_0(T) - \mathcal{K}(\tau^2)\end{aligned} \tag{39}$$

where $\Delta v = v/v_{0c} - 1$ is the dimensionless deviation of the volume from the classical critical volume v_{0c}, $\bar{P}_0(T) = P(T, v_{0c})v_{0c}/k_B T$, and $\bar{A}_0^{\mathrm{r}}(T) = A^{\mathrm{res}}(T, v_{0c})/k_B T$ are the dimensionless pressure and residual part of the Helmholtz free energy along the classical critical isochore $v = v_{0c}$, and the explicit expressions for the renormalized residual part $\bar{A}^{\mathrm{res}}(\bar{\tau}, \bar{\varphi})$, and analytical functions, $\bar{A}^{\mathrm{res}}(\bar{\tau}, 0)$ and $\bar{P}_0(\bar{\tau})$ for the classical SW EOS are given in Appendix A. The crossover SW EOS can be obtained from the crossover expression (39) by differentiation with respect to volume

$$P(T, v) = -\left(\frac{\partial A}{\partial v}\right)_T = \frac{RT}{v}\left[-\frac{v}{v_c}\left(\frac{\partial \bar{A}}{\partial \varphi}\right)_T + \frac{v}{v_{0c}}\bar{P}_0(T) + \frac{v}{v_c}\left(\frac{\partial \mathcal{K}}{\partial \varphi}\right)_T\right]. \tag{40}$$

where the kernel term $\mathcal{K}$ depends on the order parameter φ only through the argument of the crossover function $Y(q)$.

Eqs. (28)–(39) completely determine the crossover Helmholtz free energy for the SW fluids. Far away from the critical point $q \gg 1$ (or $|\tau| \gg Gi$ at $v = v_c$), the crossover function $Y(q) \to 1$, the renormalized temperature and volume tend to their classical values $\bar{\tau} \to \tau$ and $\bar{\varphi} \to \Delta v$, and Eq. (39) is transformed into the classical Helmholtz free energy density (2). Asymptotically, close to the critical point $q \ll 1$ (or $|\tau| \ll Gi$ at $v = v_c$), the crossover function $Y(q) \cong q^{\Delta_1}$, the parameters $\bar{\tau} \cong \tau q^{-(\alpha/2)}$ (or $\bar{\tau} \cong \tau^{(2-\alpha)/2}$ at $v = v_c$) and $\bar{\varphi} \cong \varphi q^{(\gamma-2\beta)/4}$, the critical part of the free energy $\Delta\bar{A}(\bar{\tau}, \bar{\varphi})$ is renormalized, and the crossover Eq. (39) for Helmholtz free energy reproduces the asymptotic scaling laws (see Eq. (26)).

4. Simulation details

Molecular dynamics (MD) simulations were performed in the NVE ensemble for 1–3 ns of simulated time. Estimating the simulated time at each temperature requires assumptions about the mass and energy of the model potentials. The mass was taken as 16 amu and the values of ϵ/k_B were taken as 146, 73, and 19 K for $\lambda = 1.5$, 2.0, 3.0, respectively. Simulations for a given potential model along a given isochore were initialized with FCC cells in accordance with the number of atoms (N) simulated in each system. Subsequent simulations along the same isochore were initialized from the final configuration of the preceding simulation with velocities rescaled to reduce the temperature. Simulated time was 3 ns for $y < 0.19$ in all cases except $\lambda = 3.0$. The long-range of the 3.0 potential resulted in slow simulations

because of the large number of neighbors. Simulated time was 1 ns for $y > 0.19$. The heat capacity of the system was estimated by regressing the values of internal energy U_r with a third-order polynomial and computing the derivative. Note that the fluctuations in compressibility factor were relatively small compared to fluctuations in temperature or internal energy. This happens because higher local temperatures induce higher local pressures. Since the pressure is in the numerator of the compressibility factor and temperature is in the denominator, their fluctuations tend to cancel.

In addition, Monte Carlo simulations were also performed for square-well fluids with $\lambda = 1.5$, 2.0, and 3. In these simulations, the system was started in a perfect face-centered cubic lattice and equilibrated using random displacements of each of the molecules. For each set of conditions, the simulations were divided into separate runs, each consisting of 10^4 attempted moves per molecule. The reported properties were taken as the average value of the runs, and the uncertainty was estimated by the standard deviation.

The simulation results are available from the authors upon request.

5. Comparisons with simulation data

The crossover EOS for SW fluids contains the following system-dependent parameters: the original classical parameters $a_j^{(i)}$ and $b_j^{(i)}$ (i, $j = 0$–3) in Eq. (2), the Gi, the critical amplitude a_{20} in the kernel term, and the sine-model parameter m_0. As mentioned above, the parameters $a_1^{(1)}$, $a_2^{(2)}$, $a_3^{(2)}$, and $b_1^{(1)}$ are directly related to the second and third virial coefficients of SW fluids and can be determined exactly (see Eqs. (14)–(17)). The coefficients $b_1^{(2)}$ and $b_1^{(3)}$ determine the behavior of the residual internal energy U_r in the limit $\beta^* \to 0$ (or, equivalently, the coefficient A'_1 in Eq. (18)).

Furthermore, since the third virial coefficients, and as a consequence the parameters $a_2^{(2)}$, $a_3^{(2)}$, and $b_1^{(1)}$ in Eq. (2), have different analytical forms in the regions $\lambda \leq 2.0$ and for $\lambda \geq 2.0$, the analytical expressions for coefficients $b_1^{(2)}$ and $b_1^{(3)}$ extracted from Eq. (2) also have different forms for $\lambda \leq 2.0$ and $\lambda \geq 2.0$ regions. Therefore, in this work the coefficients $b_1^{(2)}$ and $b_1^{(3)}$ were represented by a Taylor expansion

$$b_1^{(i)} = b_{1,0}^{(i)} + \sum_{k=1}^{4} b_{1,k}^{(i)} \Delta\lambda^k, \quad i = 2 \text{ and } 3, \tag{41}$$

where the parameter of expansion

$$\Delta\lambda = \begin{cases} \lambda - 1.5, & \text{for } \lambda \leq 2.0 \\ \lambda - 3.0, & \text{for } \lambda \geq 2.0 \end{cases} \tag{42}$$

and the coefficients $b_{1,k}^{(i)}$ for each region were found from a fit of Eq. (2) to the for hard-sphere MC simulation data for A'_1. The coefficients $b_{1,k}^{(i)}$ are listed in Table 1 and a comparison with the simulation data is given in Fig. 1. In the entire density range shown in Fig. 1 the maximum deviation of the calculated values of A'_1 from the MC simulation results is less than 0.2%, which roughly corresponds to the accuracy of the data.

Even after this elucidation, the CR EOS still contains adjustable parameters $a_j^{(i)}$ and $b_j^{(i)}$ which can be determined only from a fit of the CR EOS to the simulation data. If we also add to this number three crossover parameters Gi, a_{20}, and m_0, which in principle can dramatically change the thermodynamic

Table 1
Coefficents $b_{1,k}^{(i)}$ in Eq. (41)

Coefficient	$\lambda \leq 2$	$\lambda > 2$
$b_{1,0}^{(2)}$	1.5093018500	0.4697011630
$b_{1,1}^{(2)}$	0.9673047240	−4.604133228
$b_{1,2}^{(2)}$	6.3087619550	−26.67612171
$b_{1,3}^{(2)}$	−0.709455318	−43.58375157
$b_{1,4}^{(2)}$	−20.27785515	−19.76736755
$b_{1,0}^{(3)}$	0.5077587980	−0.528853757
$b_{1,1}^{(3)}$	−0.771042541	5.1546638240
$b_{1,2}^{(3)}$	−20.76688587	40.508756730
$b_{1,3}^{(3)}$	−12.04372937	72.750520860
$b_{1,4}^{(3)}$	61.302467810	35.181735840

description of SW fluids, it becomes clear that obtaining a reliable statistical analysis of the crossover behavior requires further restrictions on the empirical parameters. In order to obtain a representative statistical analysis of the crossover behavior of SW fluids, the number of the empirical parameters should be essentially restricted.

With this in mind, we chose the SW fluid with $\lambda = 3.0$ as our first model system. Since $Gi \propto \bar{l}_0^{-6} \propto \lambda^{-6}$, we expect that for this λ the Gi is small [53], classical MF behavior over the entire experimentally available region, and the crossover parameters a_{20}, and m_0 are statistically irrelevant. The critical amplitude a_{20}

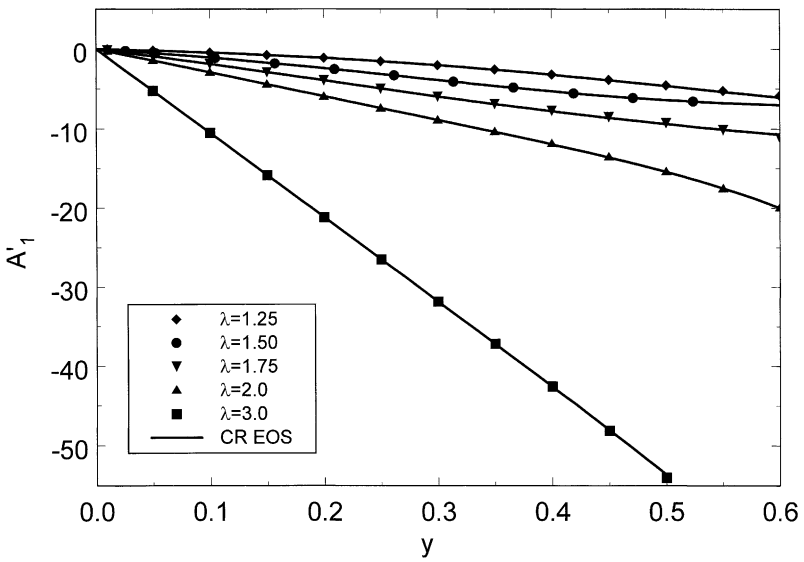

Fig. 1. Variation of A_1 with packing fraction for different square-well widths. Symbols correspond to Monte Carlo simulation results and the lines represent the values calculated with the crossover EOS.

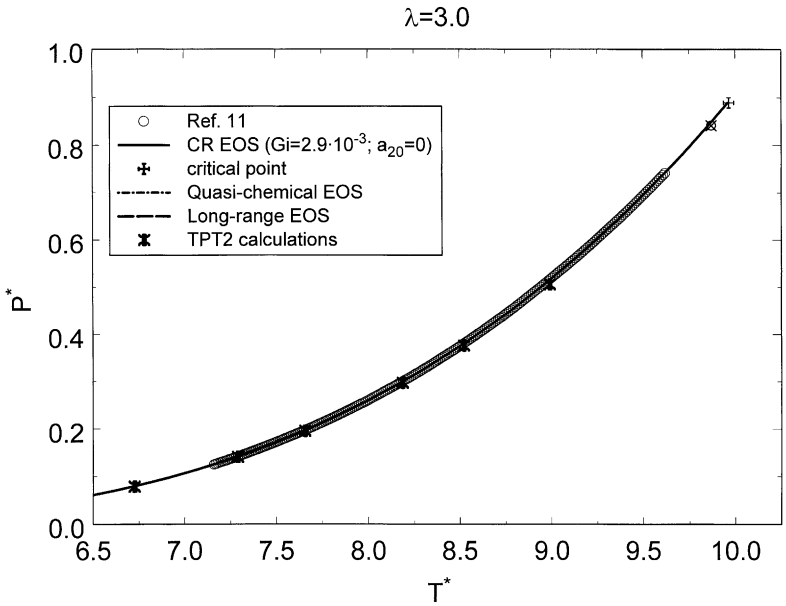

Fig. 2. Vapor pressure P^* as function of the temperature T^* for the square-well fluid with $\lambda = 3.0$. The open circles correspond to the molecular dynamic results of Orkoulas and Panagiotopoulos [11], the crossed symbols mark the critical points, the solid lines correspond to the values calculated with the crossover EOS, the dotted–dashed lines represent the values calculated with the classical quasi-chemical model (QCM) [8], the long-dashed lines correspond to the long-range approximation (LRA) [21,22], and the ants correspond to the values calculated with the second order thermodynamic perturbation theory (TPT2) [54].

determines the non-analytic singular behavior of the isochoric specific heat, which is not observed in this system, and the parameter m_0 effectively takes into account a variation of the prefactor κ in Eq. (23) for different definitions of the *Gi* [42,44], which we suppose to be small for this system. Therefore, we initially set $\Delta T_c = \Delta v_c = a_{20} = 0, m_0 = 1$, and all other parameters were found from a fit of the CR EOS to our MD and MC simulation data for the compressibility factor Z and the residual internal energy U_r in the one-phase region, and to the MC simulation VLE-data obtained by Orkoulas and Panagiotopoulos [11]. We found that the *Gi* for this system is really very small, $Gi = 2.9 \times 10^{-3}$, and that for the adequate description of all simulation data for SW fluid with $\lambda = 3.0$ only nine adjustable parameters in Eq. (2) are needed. Comparisons of the crossover model with the simulation data are given in Figs. 2–4. The average absolute deviation (ADD) between correlated and simulation data were less than 1% for both internal energy and density. For the vapor pressure, the ADD is of about 0.1% in the temperature region $7.4 \leq T^* \leq T_c^*$. At low temperatures, the deviations of the vapor pressure calculated with the CR EOS from the MC data are increased up to 0.5%.The ants in Figs. 2 and 3 correspond to the values calculated with the second-order thermodynamic perturbation theory (TPT2) [54] and the dashed lines represent the values calculated with the classical quasi-chemical model (QCM) [8] (dotted–dashed lines) and long-range approximation (LRA) [21,22] (long-dashed lines). For the vapor pressure these values are very close to the ones calculated with the CR EOS, that confirms our assumption about dominant classical behavior in this system. As one can see, the LRA and TPT2 also yield a fairly good prediction for the saturated densities in SW fluid with $\lambda = 3.0$, while the QCM predicts the much lower critical temperature in this system and, as a consequence, fails to reproduce the saturated liquid densities and the vapor densities in the critical region.

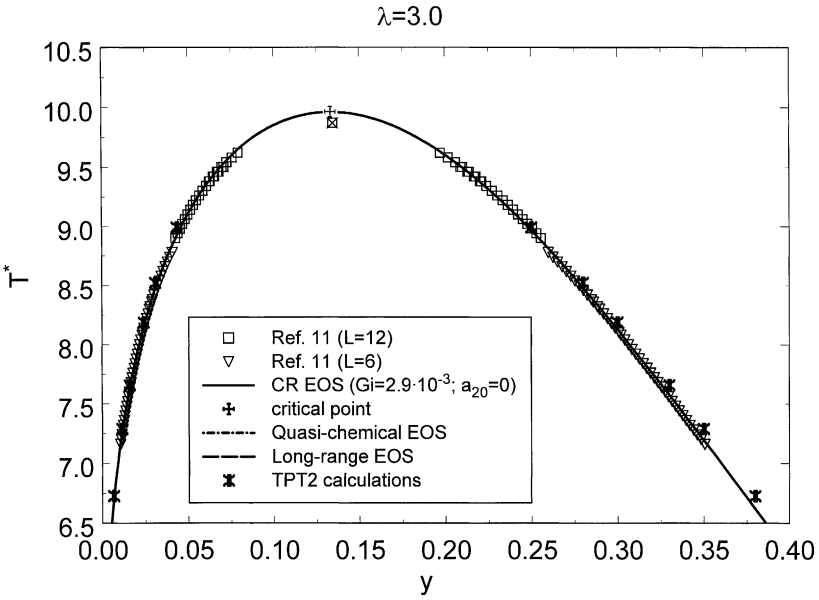

Fig. 3. Coexistence curve of the square-well fluid with $\lambda = 3.0$. The open symbols correspond to the molecular dynamic results of Orkoulas and Panagiotopoulos [11] for the system size $L = 12$ (squares) and $L = 6$ (triangles), and the other conditions are same as in Fig. 2.

As our second step, we tried to redefine the parameter a_{20} from a fit of the crossover model to the isochoric heat capacity, C_V, obtained by numerical differentiation of the molecular dynamic results for U_r. Our results for C_V are shown in Fig. 5. Incorporation of a non-zero value for a_{20} in the CR EOS for the SW fluid with $\lambda = 3.0$ does not improve description of the isochoric heat capacity far from the critical region and causes unphysical behavior at temperatures $\tau \approx Gi$. In order to avoid this unphysical behavior, the parameter a_{20}, like the Gi, should be very small. This observation confirmed our initial assumption about the predominantly classical behavior of this system. Hence, the parameter a_{20} remains zero in our best representation of this system.

The classical behavior of the SW fluid with $\lambda = 3.0$ is, in our opinion, a major reason why the critical temperature $T_c^* = 9.96$ obtained from a solution of Eq. (31) for this system differs from $T_c^* = 9.87$ obtained by Orkoulas and Panagiotopoulos [11] from the analysis of their MC simulation results. Their analysis was performed on the basis of the asymptotic scaling laws with the non-classical critical exponents as given by Eq. (27). However, it is valid only in the temperature range as given by Eq. (25). Our analysis shows, that actually all VLE-data in the critical region ($\tau \ll 1$) for the SW fluid with $\lambda = 3.0$ presented in [11] belong to the MF region as given by Eq. (24) with $\beta = 0.5$, rather than to the scaling region given by Eq. (25). As a consequence, the real critical temperature for this system is slightly higher than the critical temperature obtained by Orkoulas and Panagiotopoulos [11] from the analysis of the VLE-data with $\beta = 0.325$.

The second system considered here is the SW fluid with $\lambda = 1.5$. For the classical SW EOS, we used the same number of adjustable parameters $a_j^{(i)}$ and $b_j^{(i)}$ as in the previous case for $\lambda = 3.0$. All these parameters together with the crossover parameters Gi, a_{20}, and m_0 were found from a fit of the CR EOS

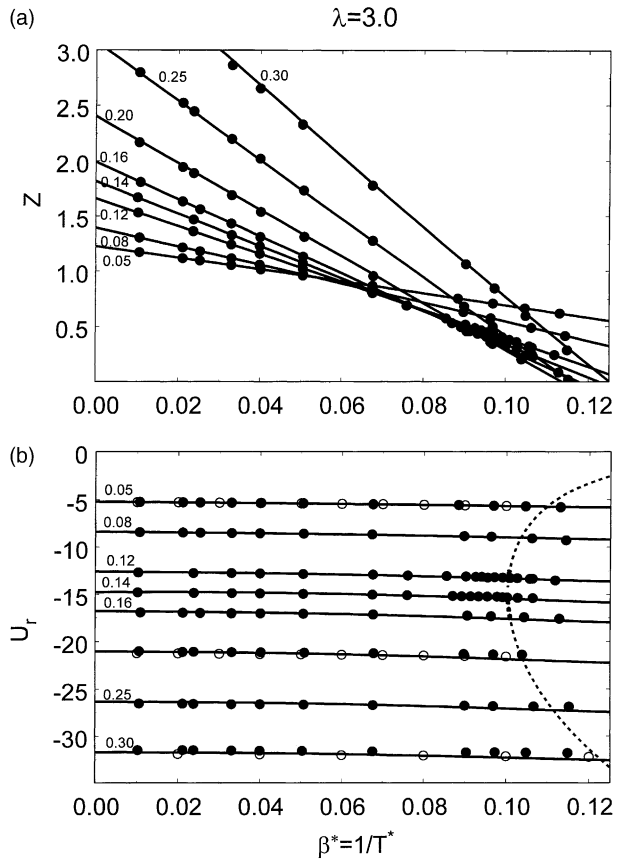

Fig. 4. Compressibility factor (a) and residual internal energy (b) along various isochores as functions of the inverse temperature $\beta^* = 1/T^*$ for the square-well fluid with $\lambda = 3.0$. The symbols correspond to the Monte Carlo (empty circles) and molecular dynamic (filled circles) results of this work for $N = 500$, and the lines represent the values calculated with the crossover EOS.

to our (Z, y, T), (U_r, y, T), and (C_V, y, T) data in the one-phase region, and VLE-data presented in [11] at condition $\Delta T_c = \Delta v_c = 0$. We found that the best description of all data is achieved with the crossover parameters

$$Gi = 0.629, \qquad a_{20} = 4.059, \qquad m_0 = 0.852. \tag{43}$$

In contrast to the previous case for $\lambda = 3.0$, the Gi for the SW fluid with $\lambda = 1.5$ is not small. Hence, the crossover contribution is essential in the region $|\tau| \leq 1$. As a consequence, the critical temperature for this system obtained from a solution of Eq. (31) with the optimized values of the parameters $a_j^{(i)}$ and $b_j^{(i)}$, $T_c^* = 1.244$, appears to be very close to $T_c^* = 1.218$ obtained by Orkoulas and Panagiotopoulos [11] from the analysis of their MD VLE-data with $\beta = 0.325$. The critical temperature reported by Orkoulas and Panagiotopolous [11] has been obtained as extrapolation of the critical temperatures for the system sizes $L = 6$, 8, and 12 to the infinite system with $L \to \infty$, while our T_c^* is a critical temperature of the real finite-size system.

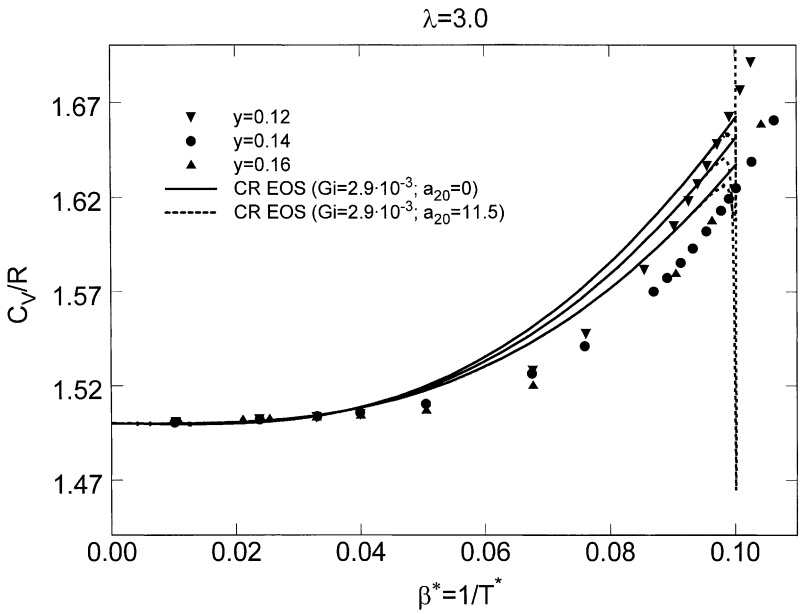

Fig. 5. Isochoric heat capacity along various isochores as function of the inverse temperature $\beta^* = 1/T^*$ for the square-well fluid with $\lambda = 3.0$. The symbols correspond to the values obtained by numerical differentiation of the molecular dynamic results for U_r presented in Fig. 4, and the lines represent the values calculated with the crossover EOS with $a_{20} = 0$ (solid lines) and with $a_{20} = 11.5$ (dashed lines).

We have also analyzed the finite-size effect of the residual internal energy U_r and the isochoric heat capacity for this system. The results of our analysis on the near-critical isochore $y = 0.16$ are shown in Figs. 10 and 11. The dashed curves in both figures represent the values calculated with the classical EOS (i.e. with the *Gi* and the critical amplitude a_{20} set to zero). The classical EOS gives qualitatively wrong behavior for the residual internal energy and the isochoric heat capacity in the critical region, while the CR EOS yields a very good representation of the simulation data up to the inverse temperature $\beta^* = 0.75$. However, in the vicinity of the critical point at $0.75 \leq \beta^* \leq 0.8$ (or $|\tau| \leq 7 \times 10^{-2}$), the finite-size effect becomes essential, and all simulation C_V data lie in this region below the values calculated with the CR EOS. Even for the system with $N = 2048$ particles, the largest system considered in this work, the systematic deviations from the asymptotic scaling behavior appear at $\Delta T \leq 0.03$ (or $|\tau| \leq 3 \times 10^{-2}$), which is the accuracy of the determination of the critical temperature from these data. It is interesting to note, that unlike the experimental data for real fluids, the simulation results do not show any jumps in U_r or C_V as the coexistence curve is crossed. They just smoothly penetrate into the metastable and even unstable regions without exhibiting any anomalies. For real fluids calorimetric data could be used to improve the accuracy of the critical temperature (see, for example, [55,56]), but the lack of divergence for simulation data of finite systems precludes application of that approach in the present instance.

In the next step, we used, for the critical shifts, Eq. (34) and redefined the coefficients $a_j^{(i)}$ and $b_j^{(i)}$ from a fit of the CR EOS to the same dataset in the temperature range $\beta^* \leq 0.75$ but with the critical temperature

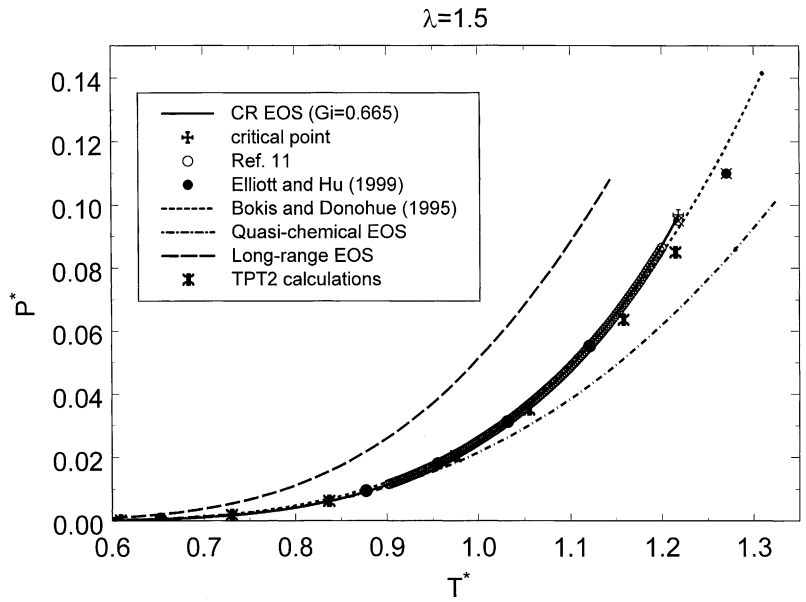

Fig. 6. Vapor pressure P^* as function of the temperature T^* for the square-well fluid with $\lambda = 1.5$. The symbols correspond to the molecular dynamic results of Orkoulas and Panagiotopoulos [11] (empty squares) and of Elliott and Hu [10] (filled circles), the crossed symbols mark the critical points for each dataset, and the short-dashed lines correspond to the values calculated with the classical Bokis–Donohue model [14], and the other conditions are same as in Fig. 2.

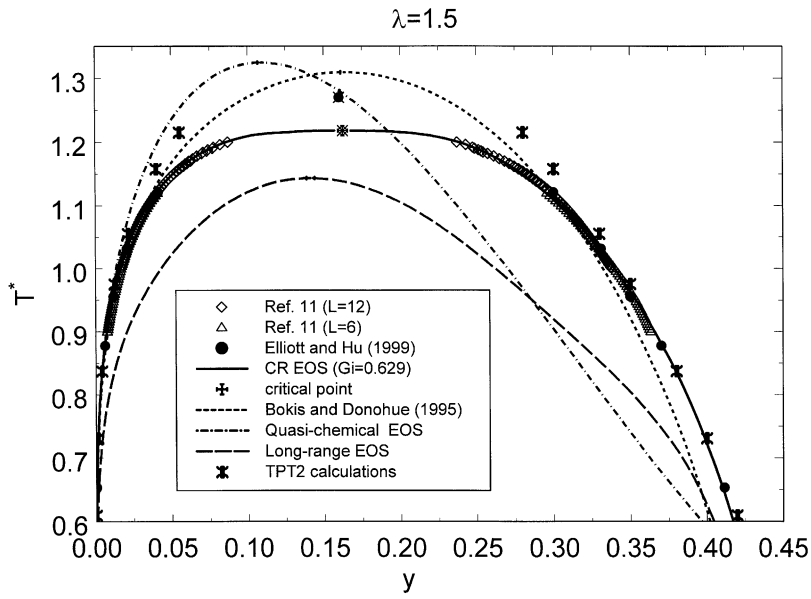

Fig. 7. Coexistence curve of the square-well fluid with $\lambda = 1.5$. The open symbols correspond to the molecular dynamic results of Orkoulas and Panagiotopoulos [11] for the system size $L = 12$ (empty diamonds) and $L = 6$ (empty triangles), and the other conditions are same as in Fig. 6.

$T_c^* = 1.218$ and the critical density $y_c = 1.623$, as proposed by Orkoulas and Panagiotopoulos [11]. With the optimized values of the coefficients $a_j^{(i)}$ and $b_j^{(i)}$ we found for $\lambda = 1.5$ the classical critical parameters $T_{c0}^* = 1.222$ and $y_{c0} = 1.554$, which in this case do not coincide with the real critical parameters T_c^* and y_c, and, with the *Gi* as given in Eq. (43), the coefficients

$$\delta_\tau = 7.82 \times 10^{-3}, \qquad \delta_\varphi = 1.11 \times 10^{-1}. \tag{44}$$

Comparisons of the crossover model with the simulation data for the SW fluid with $\lambda = 1.5$ are given in Figs. 6–9. Excellent agreement of the predictions of the CR EOS with simulation data is observed, while all classical EOS fail to reproduce the vapor pressure and saturated densities for this system in the critical region (see Figs. 6 and 7). The average deviation of the values calculated with the CR EOS

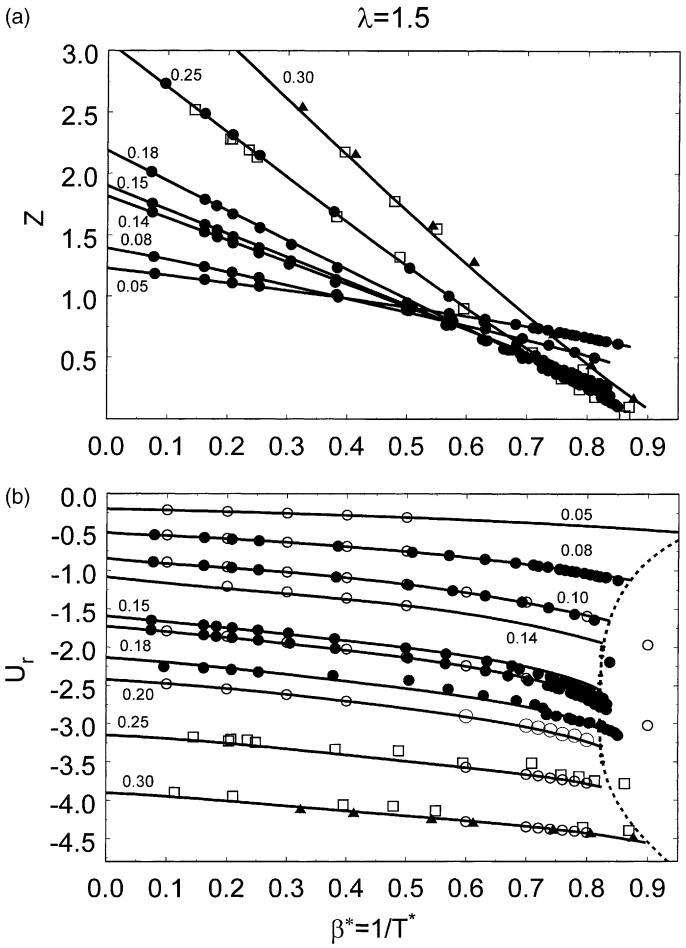

Fig. 8. Compressibility factor (a) and residual internal energy (b) along various isochores as functions of the inverse temperature $\beta^* = 1/T^*$ for the square-well fluid with $\lambda = 1.5$. The symbols correspond to the molecular dynamic results of Alder et al. [58] (empty squares), of this work for $N = 500$ (filled triangles) and $N = 2048$ (filled circles), and to the Monte Carlo results of this work for $N = 500$ (empty circles), and the lines represent the values calculated with the crossover EOS.

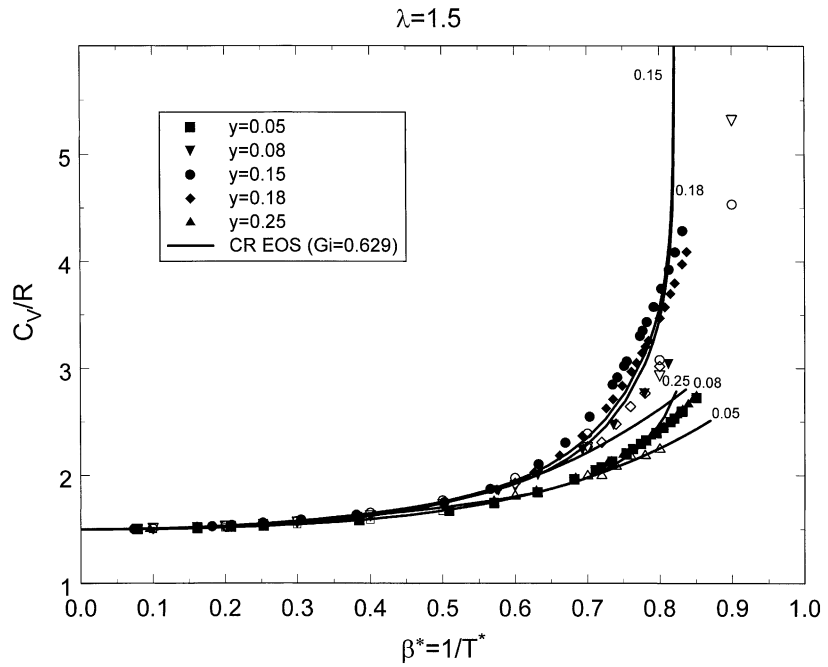

Fig. 9. Isochoric heat capacity along various isochores as function of the inverse temperature $\beta^* = 1/T^*$ for the square-well fluid with $\lambda = 1.5$. The empty symbols correspond to the Monte Carlo results of this work for $N = 500$, the filled symbols correspond to the values obtained by numerical differentiation of the molecular dynamic results for U_r presented in Fig. 8, and the lines represent the values calculated with the crossover EOS.

from simulation results is less than 1% for all properties shown in Figs. 7–11. For the vapor pressure, the average deviation is less than 0.1% (see Fig. 6).

The third system which we considered in this work is the SW fluid with $\lambda = 2.0$. Unlike the previous systems considered in this work, the VLE properties of the SW fluid with $\lambda = 2.0$ have not been as carefully studied, and the actual critical temperature and density were not established with the same accuracy as for the SW fluid with $\lambda = 1.5$. As was pointed out earlier by Kiselev and Ely [48], the coefficients δ_τ and δ_φ in Eq. (34) do not depend on the *Gi*. Therefore, in order to avoid over fitting, we used the same coefficients δ_τ and δ_φ in Eq. (34) for critical shifts for the SW fluid with $\lambda = 2.0$ as for $\lambda = 1.5$ (see Eq. (44)), and only the *Gi* was treated as an adjustable parameter. As we mentioned earlier, the parameter m_0 just renormalizes the numerical prefactor κ in Eq. (23) which depends on the path of approach to the critical point in the definition of the *Gi*, but not on the parameters of the intermolecular potential. Therefore, for this parameter, we also adopted the same value as obtained before for $\lambda = 1.5$ (see Eq. (43)), while all other parameters, including the crossover parameters

$$Gi = 0.488, \qquad a_{20} = 3.796 \tag{45}$$

were found by fitting the CR EOS to our (Z, y, T) and (U_r, y, T) data in the one-phase region, and VLE-data obtained by Elliott and Hu [10].

Fig. 12 shows the compressibility factor and residual internal energy along separate isochores as functions of the inverse temperature $\beta^* = 1/T^*$. Good agreement between calculated values and

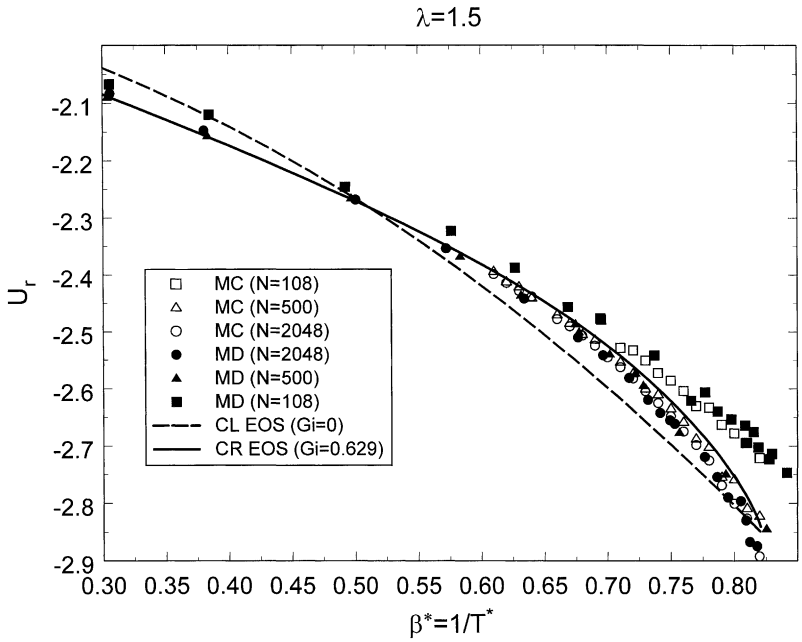

Fig. 10. Finite-size effect of the residual internal energy along the isochore $y = 0.16$ for the square-well fluid with $\lambda = 1.5$. The empty symbols correspond to the Monte Carlo results of this work for $N = 108$ (squares), $N = 500$ (triangles), and $N = 2048$ (circles), the filled symbols correspond to the molecular dynamic results of this work for the same N, and the lines represent the values calculated with the classical (dashed lines) and crossover (solid lines) EOS.

simulation data for both properties is observed. Deviations between the calculated values and simulation data in Fig. 12 are small, but at high densities ($y > 2y_c$) the isochores for the residual internal energy calculated with the CR EOS exhibit some waviness, which is physically unattractive. We do not have a complete phase diagram for the SW fluid with $\lambda = 2.0$ and, therefore, do not know for certain the location of the solid–liquid coexistence curve in this system. But if we compare $\lambda = 2.0$ fluid with the phase diagram for the Lennard–Jones (LJ) fluids obtained by Vliegenthart and Lekkerkerker [57] (see Fig. 1 in [57]), we can also assume that, similar to the LJ fluids, in the SW fluid with $\lambda = 2.0$ all data with $T^* < T_c^*$ and $y > 2y_c$ shown in Fig. 12 belong to the metastable liquid or solid phase. Future analysis of the 2.0 fluid should focus on enforcing consistency of the CR EOS with simulation data at high density, in addition to generating more simulation data along the coexistence curve.

The vapor pressure and coexistence curve simulation results obtained for the SW fluid with $\lambda = 2.0$ by Vega et al. [9] and by Elliott and Hu [10] are shown in Figs. 13 and 14. In the critical region, there is an obvious discrepancy between the two datasets. Vega et al. [9] analyzed their simulation data for the coexistence densities with the effective critical exponent $\beta = 0.53$, which is very close to the MF value $\beta_L = 0.5$, while Elliott and Hu [10] used the non-classical value $\beta = 0.325$. As a consequence, the critical temperature extracted by Vega et al. [9] from their simulation data, $T_c^* = 2.764$, is higher than the critical temperature obtained by Elliott and Hu [10], $T_c^* = 2.61$. The *Gi* for this system, $Gi = 0.488$, is slightly smaller that the *Gi* for the SW fluid with $\lambda = 1.5$ (see Eq. (43)),

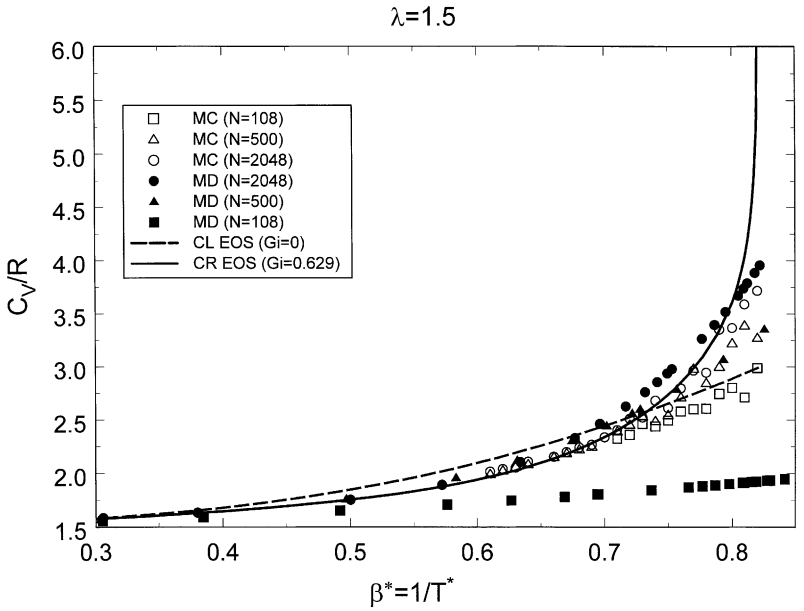

Fig. 11. Finite-size effect of the isochoric heat capacity along the isochore $y = 0.16$ for the square-well fluid with $\lambda = 1.5$. The filled symbols correspond to the values obtained by numerical dedifferentiation of the molecular dynamic results for U_r presented in Fig. 10 and the other conditions are same as in Fig. 10.

but bigger than the value $Gi = 0.111$ obtained from Eq. (23) with $\bar{l}_0/\bar{l} = \lambda = 2.0$ and $Gi_{(\lambda=1.5)} = 0.629$. Thus, for the SW fluid with $\lambda = 2.0$ the Gi ($Gi = 0.488$), is not small enough to provide a mean-field behavior in the critical region. Therefore, we would expect the critical temperature obtained by Elliott and Hu [10] to be closer to the actual value. However, the critical temperature calculated with CR EOS (i.e. $T_c^* = 2.702$) lies between the values obtained by Vega et al. [9] ($T_c^* = 2.764$) and by Elliott and Hu [10] ($T_c^* = 2.61$), while the critical density calculated with CR EOS ($y_c = 1.394$) practically coincide with the critical density obtained by Elliott and Hu [10] ($y_c = 1.40$). Similar to observations for $\lambda = 3.0$, application of $\beta = 0.50$ to the coexistence data of Elliott and Hu results in closer agreement in the critical temperature with the CR EOS but with a smaller critical density.

In order to estimate the influence of the Gi on the values of the critical parameters for SW fluid with $\lambda = 2.0$, we fit the CR EOS to the same dataset but with fixed value of $Gi = 0.112$. The result of these calculations is shown in Figs. 13 and 14 by dashed-dotted curves. In the region where the simulation data exist, both fits ($Gi = 0.488$ and $Gi = 0.112$) give practically identical results. The major difference between these two fits is in the critical region, where the CR EOS with $Gi = 0.112$ predicts a critical temperature, $T_c^* = 2.787$, which is very close to the value $T_c^* = 2.764$ obtained by Vega et al. [9]. In Fig. 15, we compare the calculated values of the isochoric heat capacity with the values obtained by numerical differentiation of the molecular dynamics results for U_r (see Fig. 12). The solid lines in Fig. 15 represent the values calculated with $Gi = 0.488$, dashed-dotted lines with $Gi = 0.112$, and the dashed lines correspond to classical EOS obtained from the CR EOS by setting $Gi = a_{20} = 0$. For the SW fluid with $\lambda = 2.0$, similar to the SW fluid with $\lambda = 1.5$, the CR EOS with small values of the Gi ($Gi = 0$

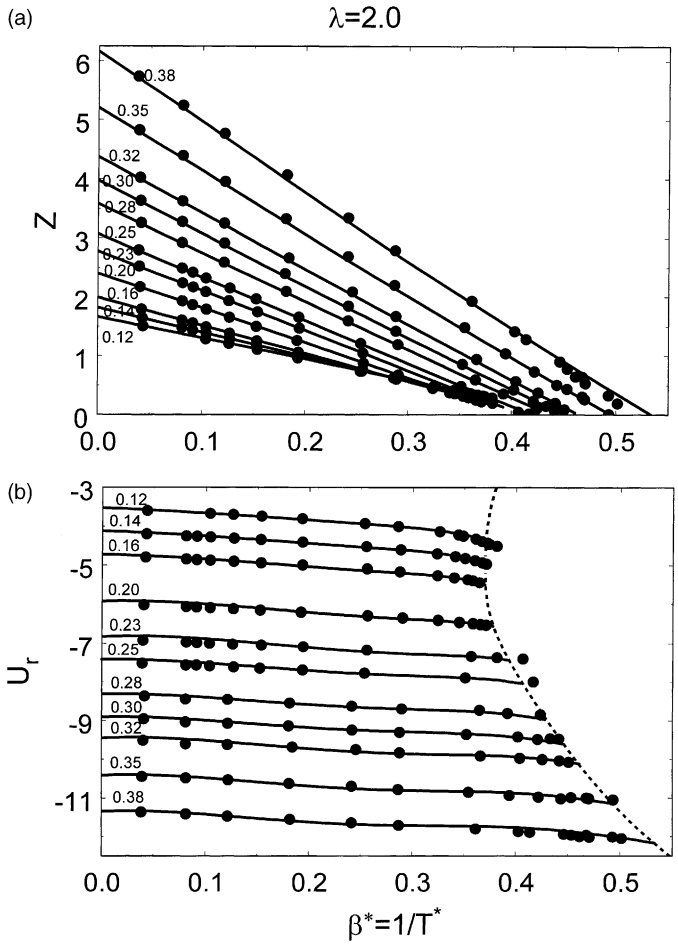

Fig. 12. Compressibility factor (a) and residual internal energy (b) along various isochores as functions of the inverse temperature $\beta^* = 1/T^*$ for the square-well fluid with $\lambda = 2.0$. The symbols correspond to the molecular dynamic results of this work for $N = 500$ and the lines represent the values calculated with the crossover EOS.

or $Gi = 0.112$) are unable to even qualitatively describe isochoric heat capacity in the critical region. In order to reproduce quantitatively the asymptotic singular behavior of the isochoric heat capacity in the critical region the *Gi* for the SW fluid with $\lambda = 2.0$, $Gi = 0.488$, should be the same order of magnitude as for the SW fluid with $\lambda = 1.5$. This conclusion is inconsistent with our estimates obtained with Eq. (23) for an ideal van der Waals fluid with $\bar{l}_0/\bar{l} = \lambda$, but is in a qualitative agreement with the independent estimates of the *Gi* for the square-well fluids obtained by Brilliantov [53].

All system-dependent coefficients in the CR EOS for SW fluids with $\lambda = 1.5$, 2.0, and 3.0 are listed in Tables 2 and 3. In Table 3, the critical parameters for SW fluids with $\lambda = 1.5$, 2.0, and 3.0 calculated with the CR EOS are compared with the critical parameters obtained by other investigators.

The computer program with the CR EOS for SW fluids with $\lambda = 1.5$, 2.0, and 3.0 is available from the authors upon request.

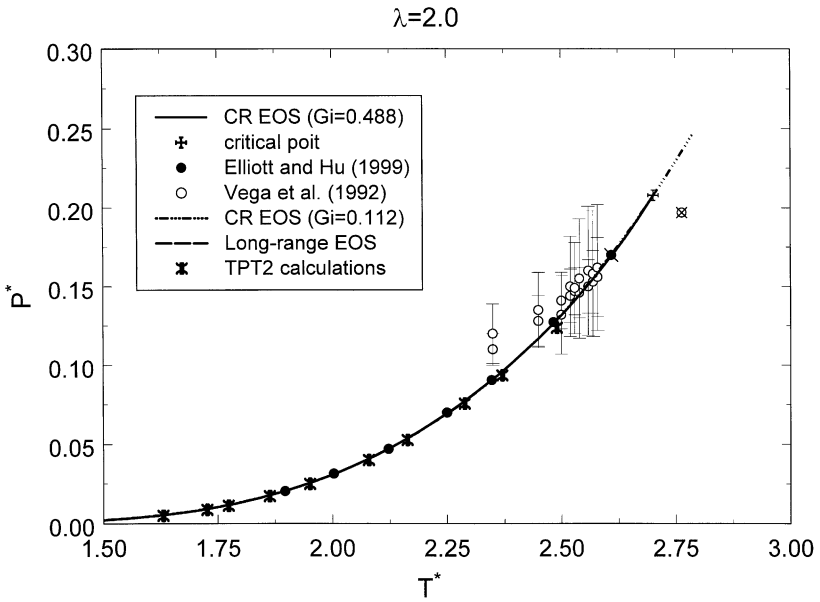

Fig. 13. Vapor pressure P^* as function of the temperature T^* for the square-well fluid with $\lambda = 2.0$. The symbols correspond to the molecular dynamic results of Vega et al. [9] (empty circles) and of Elliott and Hu [10] (filled circles), the crossed symbols mark the critical points for each dataset. The lines represent the values calculated with the crossover EOS with $Gi = 0.488$ (solid lines) and with $Gi = 0.112$ (dotted–dashed lines), with the long-range approximation (LRA) [21,22] (long-dashed lines), and the ants correspond to the values calculated with the second-order thermodynamic perturbation theory (TPT2) [54].

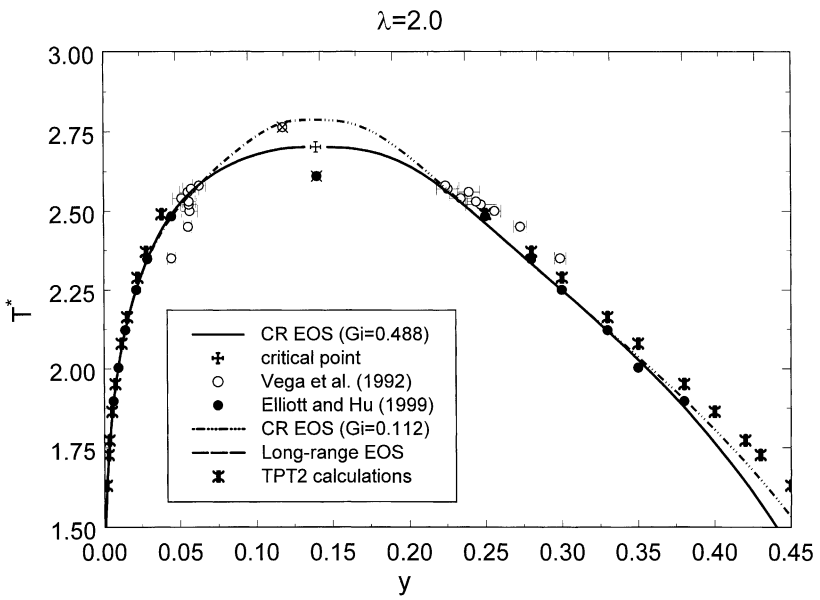

Fig. 14. Coexistence curve of the square-well fluid with $\lambda = 2.0$. Other conditions are same as in Fig. 13.

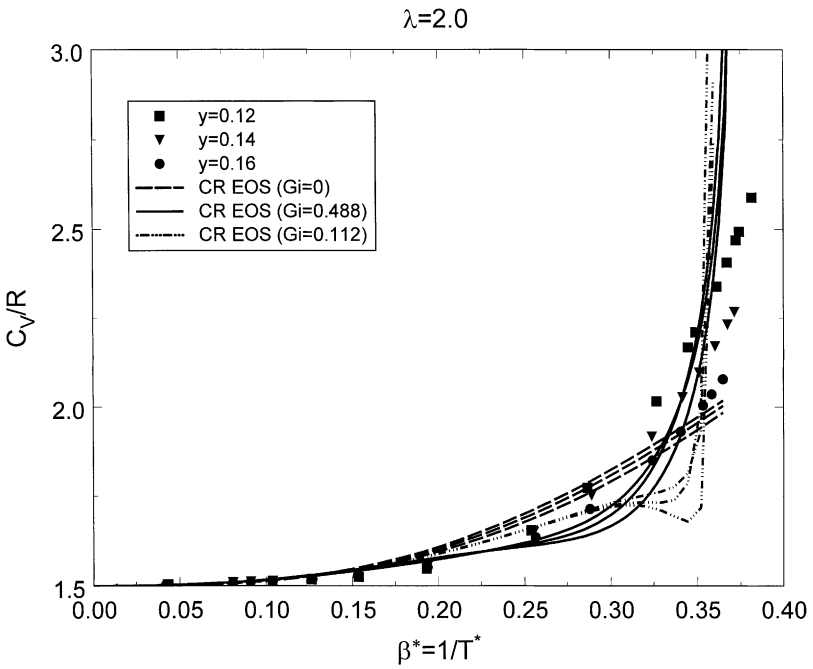

Fig. 15. Isochoric heat capacity along various isochores as function of the inverse temperature $\beta^* = 1/T^*$ for the square-well fluid with $\lambda = 2.0$. The symbols correspond to the values obtained by numerical differentiation of the molecular dynamic results for U_r presented in Fig. 12 and the lines represent the values calculated with the crossover EOS with $Gi = 0$ (long-dashed lines), with $Gi = 0.488$ (solid lines) and with $Gi = 0.112$ (dotted–dashed lines).

Table 2
System-dependent parameters for the crossover EOS

Coefficient	$\lambda = 1.5$	$\lambda = 2.0$	$\lambda = 3.0$
Classical parameters			
$a_0^{(0)}$	1.86937E+00	3.00299E+00	4.32527E+00
$a_0^{(2)}$	−1.09222E+01	1.54331E+01	5.44662E+01
$a_0^{(3)}$	5.15214E+01	2.63444E+02	−1.20356E+01
$a_0^{(5)}$	−1.17971E+02	−2.02965E+01	−5.25380E−01
$b_0^{(2)}$	−5.89252E−01	2.88015E+01	7.68267E+00
$a_2^{(3)}$	3.44813E+01	1.81800E+02	1.32461E+02
$b_2^{(2)}$	−1.29119E+01	−2.17453E+01	5.38847E−01
$b_2^{(3)}$	5.13234E+01	1.29514E+02	8.63347E+00
$a_3^{(3)}$	−1.10254E+01	−9.05033E+01	−1.18665E+03
Crossover parameters			
Gi	0.62856	0.48814	2.9×10^{-3}
a_{20}	4.05865	3.79583	0

Table 3
Critical parameterts for SW fluids

λ	Source	T_c^*	y_c	P_c^*
1.5	This work	1.218	0.162	0.097
	[11]	1.218	0.162	0.095
	[10]	1.270	0.160	0.110
	[9]	1.219	0.157	0.108
	[59]	1.215	0.167	0.097
2.0	This work	2.702	0.139	0.208
	[10]	2.610	0.140	0.170
	[9]	2.764	0.118	0.197
	[59]	2.671	0.134	0.191
	[60]	2.684	0.123	
3.0	This work	9.961	0.133	0.889
	[11]	9.871	0.135	0.841

6. Conclusions

We have performed extensive molecular dynamics and Monte Carlo simulations for square-well fluids over a range of values for λ developed a new semi-empirical crossover EOS for variable-width square-well fluids. Unlike previous equations of state, our model possess the exact second and third virial coefficients, reproduces the first high-temperature perturbation coefficient, and exhibits the correct scaling behavior in the critical regime. The parameters of our EOS were fit to our new simulation data, as well as the data of previous workers. The resulting EOS was found to provide an extremely accurate description of the thermodynamic properties of the systems we examined.

Acknowledgements

The research at the Colorado School of Mines was supported by the U.S. Department of Energy, Office of Basic Energy Sciences, under Grant no. DE-FG03-95ER41568. One of the authors (L.L.) thanks the National Institute of Standards and Technology for its financial support and hospitality.

Appendix A

The renormalized residual part of the Helmholtz free energy

$$\bar{A}^{\mathrm{res}}(\bar{\tau},\bar{\varphi}) = \frac{4\bar{y}-3\bar{y}^2}{(1-\bar{y})^2} - A_0(\bar{y})\,\ln\left[1 + A_1(\bar{y})\bar{\Delta} + A_2(\bar{y})\bar{\Delta}^2 + A_3(\bar{y})\bar{\Delta}^3\right] \tag{A.1}$$

is obtained from Eqs. (2)–(17) by replacement $\Delta \to \bar{\Delta} = \exp\{\epsilon/[k_B T_{0c}\bar{\tau}+1]\} - 1$ and $y \to \bar{y} = y_{0c}/(\bar{\varphi}+1)$, where $y_{0c} = \pi\sigma^3/6v_{0c}$. The analytic function

$$\bar{A}^{\mathrm{res}}(\bar{\tau},0) = \frac{4y_{0c}-3y_{0c}^2}{(1-y_{0c})^2} - A_0(y_{0c})\,\ln\left[1 + A_1(y_{0c})\bar{\Delta} + A_2(y_{0c})\bar{\Delta}^2 + A_3(y_{0c})\bar{\Delta}^3\right] \tag{A.2}$$

is obtained by setting $\bar{y} = y_{0c}$ in Eq. (A.1). The analytic function

$$\bar{P}_0(\bar{\tau}) = 1 - \left(\frac{\partial \bar{A}^{\mathrm{res}}}{\partial \bar{\varphi}}\right)_{\bar{\tau}(\bar{\varphi}=0)} = 1 + y_{0c}\left(\frac{\partial \bar{A}^{\mathrm{res}}(\bar{\tau},0)}{\partial y_{0c}}\right)_{\bar{\tau}} \tag{A.3}$$

is given by

$$\begin{aligned}\bar{P}_0(\bar{\tau}) = {} & \frac{1 + y_{0c} + y_{0c}^2 - y_{0c}^3}{(1-y_{0c})^3} - y_{0c}\frac{\mathrm{d}A_0}{\mathrm{d}y_{0c}}\ln(1 + A_1\bar{\Delta} + A_2\bar{\Delta}^2 + A_3\bar{\Delta}^3) \\ & - A_0\left(\frac{\mathrm{d}A_1}{\mathrm{d}y_{0c}}\bar{\Delta} + \frac{\mathrm{d}A_2}{\mathrm{d}y_{0c}}\bar{\Delta}^2 + \frac{\mathrm{d}A_3}{\mathrm{d}y_{0c}}\bar{\Delta}^3\right)(1 + A_1\bar{\Delta} + A_2\bar{\Delta}^2 + A_3\bar{\Delta}^3)^{-1}\end{aligned} \tag{A.4}$$

where

$$\frac{\mathrm{d}A_0}{\mathrm{d}y_{0c}} = \frac{2a_0^{(2)}y_{0c} + 3a_0^{(3)}y_{0c}^2 + 5a_0^{(5)}y_{0c}^4}{1 + b_0^{(2)}y_{0c}^2} - 2b_0^{(2)}\frac{a_0^{(0)}y_{0c} + a_0^{(2)}y_{0c}^3 + a_0^{(3)}y_{0c}^4 + a_0^{(5)}y_{0c}^5}{(1 + b_0^{(2)}y_{0c}^2)^2} \tag{A.5}$$

$$\begin{aligned}\frac{\mathrm{d}A_1}{\mathrm{d}y_{0c}} = {} & \frac{1}{A_0^2}\frac{\mathrm{d}A_0}{\mathrm{d}y_{0c}}\left[\frac{a_1^{(1)}y_{0c} + a_1^{(2)}y_{0c}^2 + a_1^{(3)}y_{0c}^3}{1 + b_1^{(1)}y_{0c} + b_1^{(2)}y_{0c}^2 + b_1^{(3)}y_{0c}^3}\right] + \frac{1}{A_0}\left[\frac{a_1^{(1)} + 2a_1^{(2)}y_{0c} + 3a_1^{(3)}y_{0c}^2}{1 + b_1^{(1)}y_{0c} + b_1^{(2)}y_{0c}^2 + b_1^{(3)}y_{0c}^3}\right] \\ & - \frac{1}{A_0}\left[\frac{a_1^{(1)}y_{0c} + a_1^{(2)}y_{0c}^2 + a_1^{(3)}y_{0c}^3}{(1 + b_1^{(1)}y_{0c} + b_1^{(2)}y_{0c}^2 + b_1^{(3)}y_{0c}^3)}\right](b_2^{(1)} + 2b_2^{(2)}y_{0c} + 3b_2^{(3)}y_{0c}^2)\end{aligned} \tag{A.6}$$

$$\begin{aligned}\frac{\mathrm{d}A_2}{\mathrm{d}y_{0c}} = {} & \frac{2a_2^{(2)}y_{0c} + 3a_2^{(3)}y_{0c}^2}{1 + b_2^{(1)}y_{0c} + b_2^{(2)}y_{0c}^2 + b_2^{(3)}y_{0c}^3} - \frac{a_2^{(2)}y_{0c}^2 + a_2^{(3)}y_{0c}^3}{(1 + b_2^{(1)}y_{0c} + b_2^{(2)}y_{0c}^2 + b_2^{(3)}y_{0c}^3)^2} \\ & \times (b_2^{(1)} + 2b_2^{(2)}y_{0c} + 3b_2^{(3)}y_{0c}^2)\end{aligned} \tag{A.7}$$

$$\begin{aligned}\frac{\mathrm{d}A_3}{\mathrm{d}y_{0c}} = {} & \frac{2a_3^{(2)}y_{0c} + 3a_3^{(3)}y_{0c}^2}{1 + b_3^{(1)}y_{0c} + b_3^{(2)}y_{0c}^2 + b_3^{(3)}y_{0c}^3} - \frac{a_3^{(2)}y_{0c}^2 + a_3^{(3)}y_{0c}^3}{(1 + b_3^{(1)}y_{0c} + b_3^{(2)}y_{0c}^2 + b_3^{(3)}y_{0c}^3)} \\ & \times (b_3^{(1)} + 2b_3^{(2)}y_{0c} + 3b_3^{(3)}y_{0c}^2)\end{aligned} \tag{A.8}$$

References

[1] D. Henderson, W.G. Madden, D.D. Fitts, J. Chem. Phys. 64 (1976) 5026–5034.
[2] D. Henderson, O.H. Scalise, W.R. Smith, J. Chem. Phys. 72 (1980) 2431–2438.
[3] K.-H. Lee, M. Lombardo, S.I. Sandler, Fluid Phase Equilib. 21 (1985) 177–196.
[4] M.-X. Guo, W.-C. Wang, H.-Z. Lu, Fluid Phase Equilib. 60 (1990) 37–45.
[5] M.-X. Guo, W.-C. Wang, H.-Z. Lu, Fluid Phase Equilib. 60 (1990) 221–237.
[6] D.M. Heyes, J. Phys. Cond. Mater. 2 (1990) 2241–2249.
[7] D.M. Heyes, Mol. Phys. 69 (1990) 559–569.
[8] D.M. Heyes, J. Chem. Soc., Faraday Trans. 87 (1991) 3373–3377.
[9] L. Vega, E. de Miguel, L.F. Rull, G. Jackson, I.A. McLure, J. Chem. Phys. 96 (1992) 2296–2305.

[10] J.R. Elliott, L. Hu, J. Chem. Phys. 110 (1999) 3043–3048.
[11] G. Orkoulas, A.Z. Panagiotopoulos, J. Chem. Phys. 110 (1999) 1581–1590.
[12] J.A. Barker, D. Henderson, J. Chem. Phys. 47 (1967) 2856–2861.
[13] .S. Chen, A. Kreglewski, Ber. Bunsen-Ges. Phys. Chem. 81 (1977) 1048.
[14] C.P. Bokis, M.D. Donohue, Int. J. Thermophys. 16 (1995) 1277–1286.
[15] W.R. Smith, D. Henderson, J.A. Barker, J. Chem. Phys. 55 (1971) 4027.
[16] W.R. Smith, D. Henderson, J.A. Barker, J. Chem. Phys. 64 (1976) 4244.
[17] J.A. Barker, D. Henderson, Rev. Mod. Phys. 48 (1976) 587.
[18] J. Chang, S.I. Sandler, Mol. Phys. 81 (1994) 735–744.
[19] J. Chang, S.I. Sandler, Mol. Phys. 81 (1994) 745–765.
[20] A.L. Benavides, F. del Rio, Mol. Phys. 68 (1989) 983–1000.
[21] F. del Rio, L. Lira, J. Chem. Phys. 87 (1987) 7179–7183.
[22] F. del Rio, L. Lira, Mol. Phys. 61 (1987) 275–292.
[23] R.J. Lee, K.C. Chao, Mol. Phys. 61 (1987) 1431–1442.
[24] R.J. Lee, K.C. Chao, Mol. Phys. 65 (1988) 1253–1256.
[25] K.-H. Lee, S.I. Sandler, N.C. Patel, Fluid Phase Equilib. 25 (1986) 31–39.
[26] D.A. de Lonngi, P.A. Lonngi, J. Alejandre, Mol. Phys. 71 (1990) 427–440.
[27] N.A.R. Hussain, S.M. Ahmed, J. Phys. A 24 (1991) 289.
[28] W.R. Smith, D. Henderson, R.D. Murphy, J. Chem. Phys. 61 (1974) 2911.
[29] W.R. Smith, D. Henderson, Y. Tago, J. Chem. Phys. 67 (1977) 5308.
[30] J. Bergenholtz, P. Wu, J.J. Wagner, B. d'Aguanno, Mol. Phys. 87 (1996) 331–346.
[31] L. Lue, J.M. Prausnitz, J. Chem. Phys. 108 (1998) 5529–5536.
[32] J.A. White, J. Chem. Phys. 112 (2000) 3236–3244.
[33] J.A. White, J. Chem. Phys. 113 (2000) 1580–1586.
[34] N.F. Carnahan, K.E. Starling, J. Chem. Phys. 51 (1969) 635–636.
[35] T. Kihara, Rev. Mod. Phys. 25 (1953) 831–843.
[36] C.M. Bender, S.A. Orzag, Advanced Mathematical Methods for Scientists and Engineers, McGraw-Hill, New York, 1978.
[37] L. Verlet, J.-J. Weis, Phys. Rev. A 5 (1972) 939.
[38] L.D. Landau, E.M. Lifshitz, Statistical Physics, Part 1, 3rd Edition, Pergamon Press, New York, 1980.
[39] M.E. Fisher, G. Orkoulas, Phys. Rev. Lett. 85 (2000) 696–699.
[40] A.Z. Patashinskii, V.L. Pokrovskii, Fluctuation Theory of Phase Transitions, International Series in Natural Philosophy, Pergamon Press, Oxford, 1971.
[41] J.V. Sengers, J.M.H. Levelt-Sengers, Annu. Rev. Phys. Chem. 37 (1986) 189–222.
[42] M.A. Anisimov, S.B. Kiselev, in: A.E. Scheindlin, V.E. Fortov (Eds.), Sov. Tech. Rev. B. Therm. Phys., Vol. 3, Part 2, Harwood Academic, New York, 1992, pp. 1–121.
[43] M.Y. Belyakov, S.B. Kiselev, Physica A 190 (1992) 75–94.
[44] M.A. Anisimov, S.B. Kiselev, J.V. Sengers, S. Tang, Physica A 188 (1992) 487–525.
[45] S.B. Kiselev, Fluid Phase Equilib. 147 (1998) 7–23.
[46] S.B. Kiselev, D.G. Friend, Fluid Phase Equilib. 162 (1999) 51–82.
[47] S.B. Kiselev, J.F. Ely, Ind. Eng. Chem. Res. 38 (1999) 4993–5004.
[48] S.B. Kiselev, J.F. Ely, Fluid Phase Equilib. 174 (2000) 93–113.
[49] S.B. Kiselev, High Temp. 28 (1988) 42–49.
[50] S.B. Kiselev, I.G. Kostyukova, A.A. Povodyrev, Int. J. Thermophys. 12 (1991) 877–895.
[51] A. Berestov, Sov. Phys. JETP 72 (1977) 338.
[52] M.E. Fisher, S.-Y. Zinn, P.J. Upton, Phys. Rev. B 59 (1999) 14533–14545.
[53] N.V. Brilliantov, Phys. Rev. E 58 (1998) 2628–2631.
[54] J.R. Elliott, 2001, submitted for publication.
[55] I.M. Abdulagatov, N.G. Polikhronidi, R.G. Batyrova, Ber. Bunsenges. Phys. Chem. 98 (1994) 1068–1072.
[56] I.M. Abdulagatov, B.A. Mursalov, N.M. Gamzatov, in: H. White, J.V. Sengers, D.B. Neumann, J.C. Bellows (Eds.), Physical Chemistry of Aqueous Systems, Proceedings of the 12th International Conference on the Properties of Water and Steam, Begell House, New York, 1995, pp. 94–102.
[57] G.A. Vliegenthart, H.N.W. Lekkerkerker, J. Chem. Phys. 112 (2000) 5364–5369.
[58] B.J. Alder, D.A. Young, M.A. Mark, J. Chem. Phys. 56 (1972) 3013–3029.
[59] J.A. White, Int. J. Thermophys. 22 (2001) 1147–1157.
[60] E. de Miguel, Phys. Rev. E 55 (1997) 1347–1354.